J Electr Eng Technol.2018; 13(1): 393-399
http://doi.org/10.5370/JEET.2018.13.1.393

ISSN(Print) 1975-0102
ISSN(Online) 2093-7423

Theoretical Computation of the Capacitance of an Asymmetric Coplanar Waveguide

Chan Mi Song*, Gina Kwon*, Jong Min Lee*, Kang-Yoon Lee*, Youngoo Yang* and Keum Cheol Hwang†

Abstract – An electrostatic boundary-value problem of a dielectric-wedge-backed, double-slotted conducting wedge is investigated to analyze an asymmetric coplanar waveguide with an infinite dielectric thickness using the Mellin transform and a mode-matching method. Our theoretical solution based on eigenfunction expansion and residue calculus is a rigorous and fast-convergent series form. Numerical computations are conducted to evaluate the potential field, capacitance, and characteristic impedance for various structures of the asymmetric coplanar waveguide. The computed results show good agreement with the simulated results.

Keywords: Asymmetric coplanar waveguide, Mellin transform, Mode-matching, Wedge

1. Introduction

The coplanar waveguide (CPW) has become a potential candidate in the design and manufacture of microwave integrated circuits (MICs) due to advantages such as its low dispersion, simplicity of fabrication, and straight-forward shunt and series connections without via holes [1]. In an effort to offer flexibility in the design of asymmetric integrated circuits, an asymmetric coplanar waveguide (ACPW) was investigated by Hanna and Thebault [2, 3], who utilized conformal mapping techniques. Since its introduction, various methods have been applied in the analysis of the ACPW. The propagation characteristics of the ACPW with a finite metallization thickness were investigated by combining a spectral-domain approach with a perturbation method [4]. The quasi-static parameters (the characteristic impedance and the effective dielectric constant) of the ACPW were determined based on an artificial neural network [5, 6]. A finite-difference time-domain method and a modal technique were also employed to evaluate the characteristics of the ACPW with a finite dielectric thickness [7, 8].

The purpose of the present research is to analyze an ACPW with not only asymmetric slots but also asymmetric ground planes on an infinitely thick dielectric substrate. As a continuation of earlier works [9, 10], an electrostatic boundary-value problem of a double-slotted conducting wedge with a dielectric wedge is solved to derive a rigorous solution for the ACPW using the Mellin transform and a mode-matching method. The analysis of an asymmetric coplanar waveguide (ACPW) here is obviously an extension of the work in an earlier study [10]. The present study addresses a problem associated with the ACPW, an important type of transmission line. In order to verify the validity of the proposed method, computations for the potential field, capacitance, and characteristic impedance of the ACPW are performed and the results are compared with simulated results. Details of the field representation and numerical results for the ACPW are described in the following sections.

† Corresponding Author: School of Electronic and Electrical Engineering, Sungkyunkwan University, Korea. (khwang@skku.edu)
* School of Electronic and Electrical Engineering, Sungkyunkwan University, Korea. (94chanmi@gmail.com, boo_ood@hotmail.co.kr, ljm4081@naver.com, {klee, yang09}@skku.edu)
Received: November 1, 2016; Accepted: August 16, 2017

2. Field Representation

Fig. 1(a) shows a cross-sectional view of an ACPW structure on an infinitely thick dielectric substrate ($h=\infty$) with relative permittivity ε_{2r}. A central strip conductor with a width of s is located between two asymmetric ground planes. In contrast to ACPWs considered in earlier studies [2, 3], the proposed ACPW has one finite ground plane with a width of a and a semi-infinite ground plane. Consequently, the distance of separation between the finite and semi-infinite ground planes is equal to w_1+s+w_2. In the analysis that follows, all conducting strips are assumed to have a zero thickness and perfect conductivity. In order to apply the Mellin transform and mode-matching to analyze this ACPW, we consider the boundary-value problem of a double-slotted conducting wedge with a dielectric wedge, as shown in Fig. 1(b). The electrostatic potential V is induced across an intermediate wedge section ($b\leq\rho\leq c$ and $0\leq\phi\leq\phi_0$) between two slots with an angle of ϕ_0. Note that the width of the intermediate wedge section (c-b) is equal to s and that the widths of the left and right slots are $b-a(=w_1)$ and $d-c(=w_2)$, respectively. Based on the Mellin transform [11], the electrostatic potential fields in region (I) ($\phi_0\leq\phi\leq\alpha$) and region (II) ($\alpha\leq\phi\leq 2\pi$) are represented as

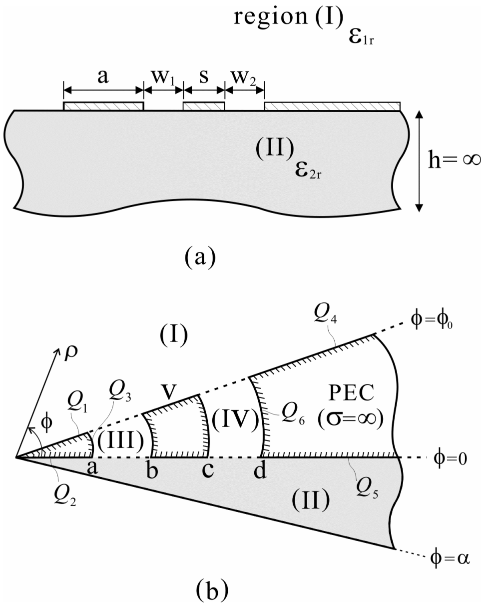

Fig. 1. (a) Asymmetric coplanar waveguide on an infinitely thick dielectric substrate, and (b) analysis model of a double-slotted conducting wedge with a dielectric wedge

$$\psi^{I}(\rho,\phi)=\frac{1}{2\pi i}\int_{c-i\infty}^{c+i\infty}\rho^{-\zeta}[\tilde{\Phi}_1(\zeta)e^{i\zeta(\phi-\phi_0)}+\tilde{\Phi}_2(\zeta)e^{-i\zeta(\phi-\phi_0)}]d\zeta \tag{1}$$

and

$$\psi^{II}(\rho,\phi)=\frac{1}{2\pi i}\int_{c-i\infty}^{c+i\infty}\rho^{-\zeta}[\tilde{\Phi}_3(\zeta)e^{i\zeta(\phi-\alpha)}+\tilde{\Phi}_4(\zeta)e^{-i\zeta(\phi-\alpha)}]d\zeta. \tag{2}$$

In the two slots (region (III): $a\le\rho\le b$ and $0\le\phi\le\phi_0$; region (IV): $c\le\rho\le d$ and $0\le\phi\le\phi_0$), the potential fields are given by the superposition principle:

$$\begin{aligned}\psi^{III}(\rho,\phi)=&\frac{2V}{\phi_0}\sum_{n=1}^{\infty}\frac{[1-(-1)^n]\sinh[\beta_n\ln(\rho/a)]}{\beta_n\sinh[\beta_n\ln(b/a)]}\sin(\beta_n\phi)\\&+\sum_{m=1}^{\infty}\sin[\phi_{m1}\ln(\rho/a)][A_m\cosh(\phi_{m1}\phi)+B_m\sinh(\phi_{m1}\phi)]\end{aligned} \tag{3}$$

and

$$\begin{aligned}\psi^{IV}(\rho,\phi)=&\frac{2V}{\phi_0}\sum_{n=1}^{\infty}\frac{[1-(-1)^n]\sinh[\beta_n\ln(\rho/d)]}{\beta_n\sinh[\beta_n\ln(c/d)]}\sin(\beta_n\phi)\\&+\sum_{m=1}^{\infty}\sin[\phi_{m2}\ln(\rho/d)][C_m\cosh(\phi_{m2}\phi)+D_m\sinh(\phi_{m2}\phi)],\end{aligned} \tag{4}$$

where $\phi_{m1}=m\pi/\ln(b/a)$, $\phi_{m2}=m\pi/\ln(c/d)$, and $\beta_n=n\pi/\phi_0$.

For the derivation of the mathematical formulas for the ACPW from the analysis model of the double-slotted conducting wedge, ϕ_0 and α are replaced with 0 and π, respectively. Field continuities at each boundary are applied to determine the unknown modal coefficients A_m, B_m, C_m, and D_m. First, the Dirichlet boundary conditions at ϕ=0, $\phi=\pi$, and $\phi=2\pi$ are enforced, as follows:

$$\psi^{I}(\rho,0)=\begin{cases}0 & \text{for } 0<\rho<a\\ \psi^{III}(\rho,0) & \text{for } a<\rho<b\\ V & \text{for } b<\rho<c\\ \psi^{IV}(\rho,0) & \text{for } c<\rho<d\\ 0 & \text{for } \rho>d\end{cases}, \tag{5}$$

$$\psi^{I}(\rho,\pi)=\psi^{II}(\rho,\pi), \tag{6}$$

and

$$\psi^{II}(\rho,2\pi)=\begin{cases}0 & \text{for } 0<\rho<a\\ \psi^{III}(\rho,0) & \text{for } a<\rho<b\\ V & \text{for } b<\rho<c\\ \psi^{IV}(\rho,0) & \text{for } c<\rho<d\\ 0 & \text{for } \rho>d\end{cases}. \tag{7}$$

Applying the Mellin transform to (5), (6), and (7) gives the following equations:

$$\begin{aligned}\tilde{\Phi}_1(\zeta)+\tilde{\Phi}_2(\zeta)=&V\frac{c^{\zeta}-b^{\zeta}}{\zeta}\\&-\sum_{m=1}^{\infty}[\phi_{m1}F_{m1}(\zeta)A_m+\phi_{m2}F_{m2}(\zeta)C_m],\end{aligned} \tag{8}$$

$$\tilde{\Phi}_1(\zeta)e^{i\zeta\pi}+\tilde{\Phi}_2(\zeta)e^{-i\zeta\pi}=\tilde{\Phi}_3(\zeta)+\tilde{\Phi}_4(\zeta), \tag{9}$$

and

$$\begin{aligned}\tilde{\Phi}_3(\zeta)e^{i\zeta\pi}+\tilde{\Phi}_4(\zeta)e^{-i\zeta\pi}=&V\frac{c^{\zeta}-b^{\zeta}}{\zeta}\\&-\sum_{m=1}^{\infty}[\phi_{m1}F_{m1}(\zeta)A_m+\phi_{m2}F_{m2}(\zeta)C_m],\end{aligned} \tag{10}$$

where $F_{m1}(\zeta)=(b^{\zeta}(-1)^m-a^{\zeta})/(\zeta^2+\phi_{m1}{}^2)$ and $F_{m2}(\zeta)=(d^{\zeta}-c^{\zeta}(-1)^m)/(\zeta^2+\phi_{m2}{}^2)$. Next, we employ the Neumann boundary conditions of

$$\varepsilon_{1,2}\left.\frac{\partial\psi^{I,II}}{\partial\phi}\right|_{\phi=0,2\pi}=\varepsilon_3\left.\frac{\partial\psi^{III}}{\partial\phi}\right|_{\phi=0}\quad\text{for } a<\rho<b, \tag{11}$$

$$\varepsilon_1\left.\frac{\partial\psi^{I}}{\partial\phi}\right|_{\phi=\pi}=\varepsilon_2\left.\frac{\partial\psi^{II}}{\partial\phi}\right|_{\phi=\pi}\quad\text{for } 0<\rho<\infty, \tag{12}$$

and

$$\varepsilon_{1,2}\left.\frac{\partial\psi^{I,II}}{\partial\phi}\right|_{\phi=0,2\pi}=\varepsilon_4\left.\frac{\partial\psi^{IV}}{\partial\phi}\right|_{\phi=0}\quad\text{for } c<\rho<d. \tag{13}$$

Accounting for the field orthogonality

($\int_a^b \rho^{-1}\sin(\phi_{p1}\ln(\rho/a))d\rho$ or $\int_c^d \rho^{-1}\sin(\phi_{p2}\ln(\rho/d))d\rho$) to (11) and (13) results in four sets of simultaneous equations:

$$\sum_{m=1}^{\infty} A_m\phi_{m1}\phi_{p1}I_1 \mp \sum_{m=1}^{\infty} B_m \frac{\varepsilon_3\phi_{m1}\chi_{mp}^1}{\varepsilon_{1,2}} + \sum_{m=1}^{\infty} C_m\phi_{m2}\phi_{p1}I_2 = V\phi_{p1}I_{s1} \tag{14}$$

and

$$\sum_{m=1}^{\infty} A_m\phi_{m1}\phi_{p2}I_3 + \sum_{m=1}^{\infty} C_m\phi_{m2}\phi_{p2}I_4 \mp \sum_{m=1}^{\infty} D_m \frac{\varepsilon_4\phi_{m2}\chi_{mp}^2}{\varepsilon_{1,2}} = V\phi_{p2}I_{s2}, \tag{15}$$

where

$$\chi_{mp}^1 = \begin{cases} \ln\sqrt{b/a} & \text{if } m = p \\ 0 & \text{if } m \neq p \end{cases}, \tag{16}$$

$$\chi_{mp}^2 = \begin{cases} \ln\sqrt{d/c} & \text{if } m = p \\ 0 & \text{if } m \neq p \end{cases}, \tag{17}$$

$$I_{1,2} = \frac{1}{2\pi i}\int_{c-i\infty}^{c+i\infty} \zeta F_{m1,m2}(\zeta)F_{p1}(-\zeta)[\csc(\zeta 2\pi) - \cot(\zeta 2\pi)]d\zeta, \tag{18}$$

$$I_{3,4} = \frac{1}{2\pi i}\int_{c-i\infty}^{c+i\infty} \zeta F_{m1,m2}(\zeta)F_{p2}(-\zeta)[\csc(\zeta 2\pi) - \cot(\zeta 2\pi)]d\zeta, \tag{19}$$

and

$$I_{s1,s2} = \frac{1}{2\pi i}\int_{c-i\infty}^{c+i\infty} [c^{\zeta} - b^{\zeta}]F_{p1,p2}(-\zeta)[\csc(\zeta 2\pi) - \cot(\zeta 2\pi)]d\zeta. \tag{20}$$

It is important to note that the integral (18)-(20) can be converted into the fast-convergent series using residue calculus, as follows:

$$I_1 = \frac{i}{2\phi_{m1}}\ln\left(\frac{b}{a}\right)\frac{1-\cos(i\phi_{m1}2\pi)}{\sin(i\phi_{m1}2\pi)}\delta_{mp} - \frac{1}{\pi}\sum_{v=1}^{\infty}\zeta_v G(\zeta_v)\frac{1-(a/b)^{\zeta_v}(-1)^p}{(\zeta_v{}^2+\phi_{m1}{}^2)(\zeta_v{}^2+\phi_{p1}{}^2)}, \tag{21}$$

$$I_{2,3} = -\frac{1}{2\pi}\sum_{v=1}^{\infty}\zeta_v G(\zeta_v)F_{p1,m1}(\zeta_v)F_{m2,p2}(-\zeta_v), \tag{22}$$

$$I_4 = \frac{i}{2\phi_{m2}}\ln\left(\frac{d}{c}\right)\frac{1-\cos(i\phi_{m2}2\pi)}{\sin(i\phi_{m2}2\pi)}\delta_{mp} - \frac{1}{\pi}\sum_{v=1}^{\infty}\zeta_v G(\zeta_v)\frac{1-(c/d)^{\zeta_v}(-1)^m}{(\zeta_v{}^2+\phi_{m2}{}^2)(\zeta_v{}^2+\phi_{p2}{}^2)}, \tag{23}$$

and

$$I_{s1,s2} = \pm\frac{1}{2\pi}\sum_{v=1}^{\infty} G(\zeta_v)(c^{\mp\zeta_v} - b^{\mp\zeta_v})F_{p1,p2}(\pm\zeta_v), \tag{24}$$

where $G(\zeta) = \sec(\zeta 2\pi) - 1$ and $\zeta_v = (2v-1)/2$. The electrostatic potential fields in regions (I) and (II) are then represented in a series form after solving (14) and (15) for the unknown modal coefficients (A_m, B_m, C_m, and D_m), as follows:

$$\psi^{I,II}(\rho,\phi) = [I_a(\rho,\phi) - I_b(\rho,\phi)] - \sum_{m=1}^{\infty}[A_m\phi_{m1}I_c(\rho,\phi) + C_m\phi_{m2}I_d(\rho,\phi)], \tag{25}$$

where $\zeta_t = t/2$,

$$I_a(\rho,\phi) = \begin{cases} V + \dfrac{V}{2\pi}\displaystyle\sum_{t=1}^{\infty}\left(\frac{c}{\rho}\right)^{-\zeta_t}\frac{K(\phi)}{\zeta_t} & \text{for } 0<\rho<c \\ -\dfrac{V}{2\pi}\displaystyle\sum_{t=1}^{\infty}\left(\frac{c}{\rho}\right)^{\zeta_t}\frac{K(\phi)}{\zeta_t} & \text{for } \rho>c \end{cases}, \tag{26}$$

$$I_b(\rho,\phi) = \begin{cases} V + \dfrac{V}{2\pi}\displaystyle\sum_{t=1}^{\infty}\left(\frac{b}{\rho}\right)^{-\zeta_t}\frac{K(\phi)}{\zeta_t} & \text{for } 0<\rho<b \\ -\dfrac{V}{2\pi}\displaystyle\sum_{t=1}^{\infty}\left(\frac{b}{\rho}\right)^{\zeta_t}\frac{K(\phi)}{\zeta_t} & \text{for } \rho>b \end{cases}, \tag{27}$$

$$I_c(\rho,\phi) = -\frac{1}{2\pi}\sum_{t=1}^{\infty}K(\phi)\frac{(b/\rho)^{-\alpha\zeta_t}(-1)^m - (a/\rho)^{-\beta\zeta_t}}{\zeta_t{}^2+\phi_{m1}{}^2} + \frac{\alpha-\beta}{2} \times \frac{\sinh(\phi_{m1}\phi) - \sinh(\phi_{m1}(\phi-2\pi))}{\phi_{m1}\sinh(\phi_{m1}2\pi)}(-1)^m\sin(\phi_{m1}\ln(b/\rho)), \tag{28}$$

$$\begin{cases} \alpha=1,\ \beta=1 & \text{for } 0<\rho<a \\ \alpha=1,\ \beta=-1 & \text{for } a<\rho<b, \\ \alpha=-1,\ \beta=-1 & \text{for } \rho>b \end{cases} \tag{29}$$

$$I_d(\rho,\phi) = -\frac{1}{2\pi}\sum_{t=1}^{\infty}K(\phi)\frac{(d/\rho)^{-q\zeta_t} - (c/\rho)^{-l\zeta_t}(-1)^m}{\zeta_t{}^2+\phi_{m2}{}^2} + \frac{q-l}{2} \times \frac{\sinh(\phi_{m2}\phi) - \sinh(\phi_{m2}(\phi-2\pi))}{\phi_{m2}\sinh(\phi_{m2}2\pi)}\sin(\phi_{m2}\ln(d/\rho)), \tag{30}$$

$$\begin{cases} q=1,\ l=1 & \text{for } 0<\rho<c \\ q=1,\ l=-1 & \text{for } c<\rho<d, \\ q=-1,\ l=-1 & \text{for } \rho>d \end{cases} \tag{31}$$

and

$$K(\phi) = \frac{\sin(\zeta_t\phi) - \sin(\zeta_t(\phi-2\pi))}{\cos(\zeta_t 2\pi)}. \tag{32}$$

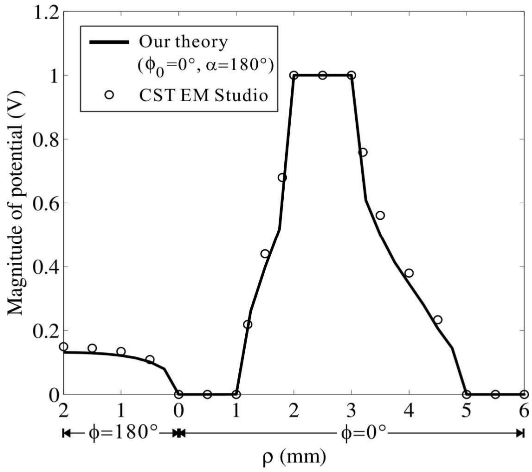

(a)

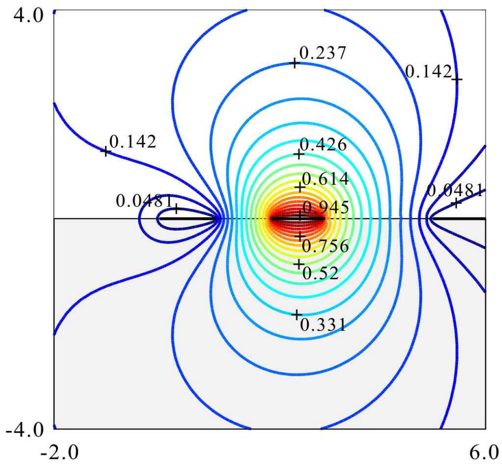

(b)

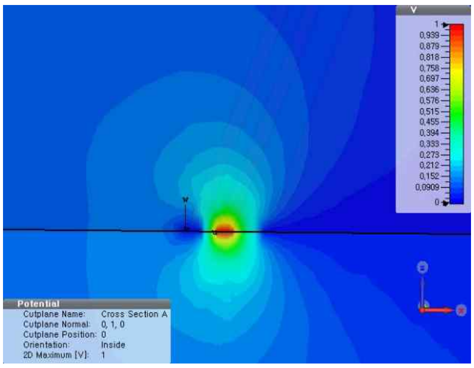

(c)

Fig. 2. (a) Magnitude of the potential on an aperture; (b) computed and (c) simulated equipotential contour of an ACPW when a=1.0 mm, s=1.0 mm, w_1=1.0 mm, w_2=2.0 mm, $\varepsilon_{1r}=\varepsilon_{3r}=\varepsilon_{4r}$=1.0, and ε_{2r}=2.0

3. Numerical Results

In order to show the validation of our theoretical solution, numerical computations are performed for various structures of the ACPW. Fig. 2(a) shows the computed and simulated results for the magnitude of the potential field on an aperture of the ACPW ($\phi_0=0^\circ$). Our theoretical result is in good agreement with the simulated result using EM Studio of CST [12]. There are twenty seven modes m used in this computation, indicating that the derived series solution is fast-convergent and numerically efficient. Fig. 2(b) illustrates the equipotential contour of the electrostatic field of the ACPW with the same parameters used in Fig. 2(a). It can be observed that the potential field is continuous across the slot apertures and is concentrated around the central strip.

The normalized per-unit length capacitance C of the ACPW is obtained from the charge accumulations of a dielectric-wedge-backed, double-slotted conducting wedge with ϕ_0=0 and $\alpha=\pi$, as illustrated in Fig. 1. C is then defined as $(Q_1+Q_2+Q_4+Q_5)/(VL)$, where L is the length of the wedge along the z-direction. Here, the charge accumulations Q_3 and Q_6 are zero because we assumed that the conducting strips of the ACPW have a zero thickness. Using the potential fields derived in the previous section, the charge accumulations of the ACPW are expressed as series form:

$$Q_{1,2}\Big|_{\phi_0=0,\alpha=\pi}=\varepsilon_{1,2}L\left\{\begin{array}{l}\dfrac{V}{2\pi}\displaystyle\sum_{t=1}^{\infty}\left[\left(\frac{a}{b}\right)^{\zeta_t}-\left(\frac{a}{c}\right)^{\zeta_t}\right]\frac{G(\zeta_t)}{\zeta_t}\\ -\displaystyle\sum_{m=1}^{\infty}\left[\begin{array}{l}\dfrac{\phi_{m1}A_m}{2\pi}\displaystyle\sum_{t=1}^{\infty}a^{\zeta_t}F_{m1}(-\zeta_t)G(\zeta_t)\\ +\dfrac{\phi_{m2}C_m}{2\pi}\displaystyle\sum_{t=1}^{\infty}a^{\zeta_t}F_{m2}(-\zeta_t)G(\zeta_t)\end{array}\right]\end{array}\right\} \tag{33}$$

and

$$Q_{4,5}\Big|_{\phi_0=0,\alpha=\pi}=\varepsilon_{1,2}L\left\{\begin{array}{l}-\dfrac{V}{2\pi}\displaystyle\sum_{t=1}^{\infty}\left[\left(\frac{b}{d}\right)^{\zeta_t}-\left(\frac{c}{d}\right)^{\zeta_t}\right]\frac{G(\zeta_t)}{\zeta_t}\\ -\displaystyle\sum_{m=1}^{\infty}\left[\begin{array}{l}\dfrac{\phi_{m1}A_m}{2\pi}\displaystyle\sum_{t=1}^{\infty}d^{-\zeta_t}F_{m1}(\zeta_t)G(\zeta_t)\\ +\dfrac{\phi_{m2}C_m}{2\pi}\displaystyle\sum_{t=1}^{\infty}d^{-\zeta_t}F_{m2}(\zeta_t)G(\zeta_t)\end{array}\right]\end{array}\right\}. \tag{34}$$

The computed, normalized per-unit length capacitance of the ACPW versus the width s of the central strip is depicted in Fig. 3 when the relative permittivity of the dielectric substrate (ε_{2r}) varies from 2.0 to 10.0. This figure shows that the capacitance increases as the strip width s or the value of ε_{2r} increases. There is also good agreement between the computation and simulation results, and relative errors between these results are approximately 5%. CST EM STUDIO cannot calculate the capacitance directly. It computes total charge accumulations. The simulated capacitance was therefore computed using the equation $C=Q_{\text{total}}/(VL)$. Some discrepancies between the computation and simulation results can be attributed to

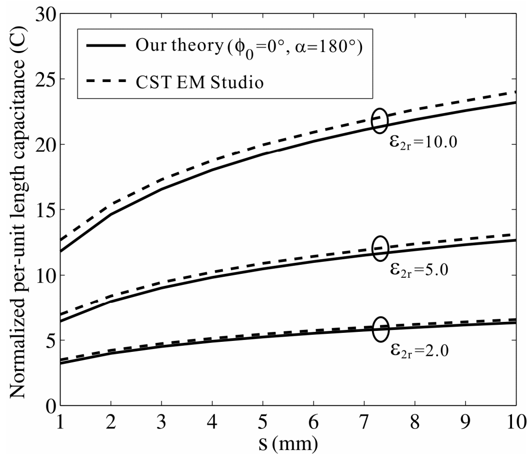

Fig. 3. Normalized per-unit length capacitance of an ACPW versus s when a=20.0 mm, w_1=1.0 mm, w_2=2.0 mm, ε_{1r}=ε_{3r} =ε_{4r} =1.0, and ε_{2r}=2.0, 5.0, or 10.0

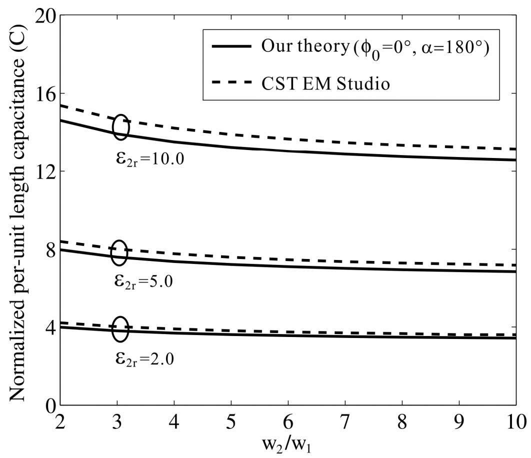

Fig. 4. Normalized per-unit length capacitance of an ACPW versus w_2/w_1 when a=20.0 mm, s=2.0 mm, ε_{1r}=ε_{3r} =ε_{4r} =1.0, and ε_{2r}=2.0, 5.0, or 10.0

the fact that the CST EM simulation uses a three-dimensional ACPW structure with a finite width, whereas the computation uses an ACPW with an infinite width. We simulated a finite structure that was sufficiently thick and long enough to compare the result using a mode-matching technique. We also applied an open boundary condition on the $X_{\min}$ and $Z_{\min}$ boundaries and an open-add boundary condition on other boundaries. Fig. 4 shows the capacitance behavior with respect to the asymmetry ratio w_2/w_1 of the ACPW for three different values of ε_{2r}. The slot asymmetry leads to a slight decrease in the capacitance, but the capacitance converges as the asymmetry ratio w_2/w_1 exceeds 6.

Fig. 5 illustrates the results of the characteristic impedance of the ACPW with different relative permittivities of the dielectric substrate (ε_{2r}=2.0, 5.0, or 10.0) versus the width s of the central strip. In a frequency-dependent analysis, the

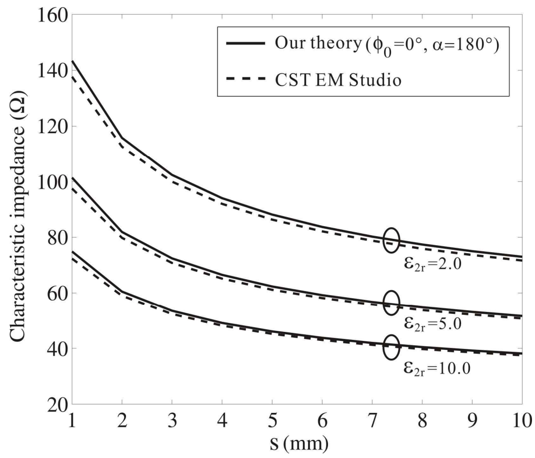

Fig. 5. Characteristic impedance of an ACPW versus s when a=20.0 mm, w_1=1.0 mm, w_2=2.0 mm, ε_{1r}=ε_{3r} =ε_{4r} =1.0, and ε_{2r}=2.0, 5.0, or 10.0

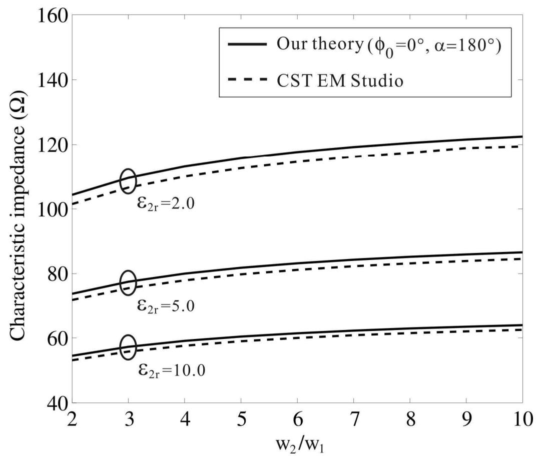

Fig. 6. Characteristic impedance of an ACPW versus w_2/w_1 when a=20.0 mm, s=2.0 mm, ε_{1r}=ε_{3r} =ε_{4r} =1.0, and ε_{2r}=2.0, 5.0, or 10.0

characteristic impedance of the CPW with coupled slots is usually defined as power-voltage ratio:

$$Z_0 = \frac{V_0}{P_{avg}}, \tag{35}$$

where V_0 is the slot voltage and P_{avg} is the time-averaged power flow on the slot line. In a quasi-static analysis, however, the characteristic impedance of the ACPW is derived from the computed capacitance due to the difficulty encountered when calculating the time-averaged power in (35):

$$Z_0 = \left(c\sqrt{CC^a}\right)^{-1}. \tag{36}$$

Here, c is the velocity of light in free space and C^a is the capacitance of the ACPW when the dielectric substrate is air (ε_{2r}=1.0).

As shown in the figure, an increase in the width s results in a decrease of the characteristic impedance for all material cases. The effect of the asymmetry ratio w_2/w_1 on the characteristic impedance can be found in Fig. 6. The characteristic impedance of the ACPW with w_2/w_1=10 increased by almost 15% compared to the case of w_2/w_1=2.

4. Conclusion

In this article, a fast-convergent series solution for the electrostatic potential field of an ACPW is investigated based on the Mellin transform and a mode-matching method. The capacitance and characteristic impedance are analytically computed by the derived series, and the effects for the width of a signal line and slot asymmetry are discussed. The computed results demonstrate that our theoretical formulations are rigorous and numerically efficient for evaluating the quasi-static characteristics of ACPWs. Therefore, the proposed static solution is useful for analyses of various ACPWs.

Acknowledgements

This work was supported by the National Research Foundation of Korea (NRF) grant funded by the Korean government (MSIP) (2014R1A5A1011478).

References

[1] R. N. Simons, Coplanar waveguide circuits, components, and systems, New York: Wiley, 2001.

[2] V. F. Hanna and D. Thebault, "Analysis of asymmetrical coplanar waveguides," *Int. J. Electron*., vol. 50, no. 3, pp. 221-224, Feb. 1981.

[3] V. F. Hanna and D. Thebault, "Theoretical and experimental investigation of asymmetric coplanar waveguides," *IEEE Trans. Microw. Theory Tech*., vol. MTT-32, no. 12, pp. 1649-1651, Dec. 1984.

[4] T. Kitazawa and T. Itoh, "Propagation characteristics of coplanar-type transmission lines with lossy media," *IEEE Trans. Microw. Theory Tech*., vol. 39, no. 10, pp. 1694-1700, Oct. 1991.

[5] E. D. Ubeyli and I. Guler, "Multilayer perceptron neural networks to compute quasistatic parameters of asymmetric coplanar waveguides," *Neurocomputing*, vol. 62, pp. 349-365, Dec. 2004.

[6] C. Yildiz, S. Sagiroglu, and O. Saracoglu, "Neural models for coplanar waveguides with a finite dielectric thickness," *Int. J. RF Microw. Comput-Aid. Eng*., vol. 13, no. 6, pp. 438-446, Nov. 2003.

[7] C. Peng, S.-J. Fang, and W. En-cheng, "Analysis of characteristic impedance of asymmetric coplanar waveguide using finite-difference time-domain method," *IEEE International Symposium on MAPE, Beijing, China*, pp. 91-94, Aug. 2005.

[8] A. Khodja, D. Abbou, M. C. E. Yagoub, R. Touhami, and H. Baudrand, "Novel dispersive modal approach for fast analysis of asymmetric coplanar structures on isotropic/anisotropic substrates," *J. Electromagn. Waves Appl*., vol. 28, no. 12, pp. 1522-1540, Jul. 2014.

[9] G. Kwon and K. C. Hwang, "Capacitance computation of coplanar waveguide using the Mellin transform and mode-matching," *IEEE Microw. Wireless Compon. Lett*., vol. 22, no. 8, pp. 385-387, Aug. 2012.

[10] G. Kwon, K. C. Hwang, Y. Yang, and K.-Y. Lee, "Mellin transform approach for the capacitance computation of asymmetric coplanar striplines," *Electromagnetics*, vol. 34, no. 8, pp. 617-624, Oct. 2014.

[11] H. J. Eom, "Integral transforms in electromagnetic formulation," *J. Electromagn. Eng. Sci*., vol. 14, no. 3, pp. 273-277, Sep. 2014.

[12] Computer Simulation Technology (CST). EM Studio [Online]. Available: http://www.cst.com

Chan Mi Song received her B.S degree in Electronics and Electrical Engineering from Dongguk University, Seoul, South Korea in 2015. She is currently working toward the combined M.S and Ph.D degree in electronic and electrical at Sungkyunkwan University, Suwon, South Korea. Her research interests include theoretical electromagnetics and electromagnetic scattering/radiation.

Gina Kwon received her B.S. degree in Electronics Engineering from Dongguk University, Seoul, South Korea in 2012. She is currently working toward her Ph.D degree in electronic and electrical engineering at Sungkyunkwan University, Suwon, South Korea. Her research interests include phased array antenna and optimization algorithms for electromagnetic applications.

Jong Min Lee received his B.S. degree in Electronics Engineering from Dongguk University, Seoul, South Korea in 2014. He is currently working toward his Ph.D degree in electronic and electrical engineering at Sungkyunkwan University. His research interests analysis and design of multi-band, wideband, array antennas.

Kang-Yoon Lee received the B.S. M.S., and Ph.D. degrees in the School of Electrical Engineering from Seoul National University, Seoul, Korea, in 1996, 1998, and 2003, respectively. From 2003 to 2005, he was with GCT Semiconductor Inc., San Jose, CA, where he was a Manager of the Analog Division and worked on the design of CMOS frequency synthesizer for CDMA/PCS/PDC and single-chip CMOS RF chip sets for W-CDMA, WLAN, and PHS. From 2005 to 2011, he was with the Department of Electronics Engineering, Konkuk University as an Associate Professor. Since 2012, he has been with School of Information and Communication Engineering, Sungkyunkwan University, where he is currently an Associate Professor. His research interests include implementation of power integrated circuits, CMOS RF transceiver, analog integrated circuits, and analog/digital mixed-mode VLSI system design.

Youngoo Yang received the Ph.D. degree in electrical and electronic engineering from the Pohang University of Science and Technology (Postech), Pohang, Korea, in 2002. From 2002 to 2005, he was with Sky works Solutions Inc., Newbury Park, CA, where he designed power amplifiers for various cellular handsets. Since March 2005, he has been with the School of Information and Communication Engineering, Sungkyunkwan University, Suwon, Korea, where he is currently a professor. His research interests include RF/mm-wave power amplifiers, RF transmitters, and DC-DC converters.

Keum Cheol Hwang received his B.S. in Electronics Engineering degree from Pusan National University, Busan, South Korea in 2001. He then received his M.S. and Ph.D. in Electrical and Electronics Engineering degrees from KAIST, Daejeon, South Korea in 2003 and 2006, respectively. He was a senior research engineer at Samsung Thales, Yongin, South Korea from 2006 to 2008, where he was involved in the development of different antennas, including multiband fractal antennas for communication systems, Cassegrain reflector antennas, and slotted waveguide arrays for tracking radars. He was an associate professor at the Division of Electronics and Electrical Engineering, Dongguk University, Seoul, South Korea from 2008 to 2014. He joined the Department of Electronic and Electrical Engineering, Sungkyunkwan University, Suwon, South Korea in 2015, where he is now an associate professor. His research interests include advanced electromagnetic scattering, radiation theory, and applications, design of multi-band/broadband and radar antennas, and optimization algorithms for electromagnetic applications. Prof. Hwang is a lifetime member of KIEES, a senior member of IEEE, and a member of IEICE.